Journal of Materials Chemistry A

Accepted Manuscript

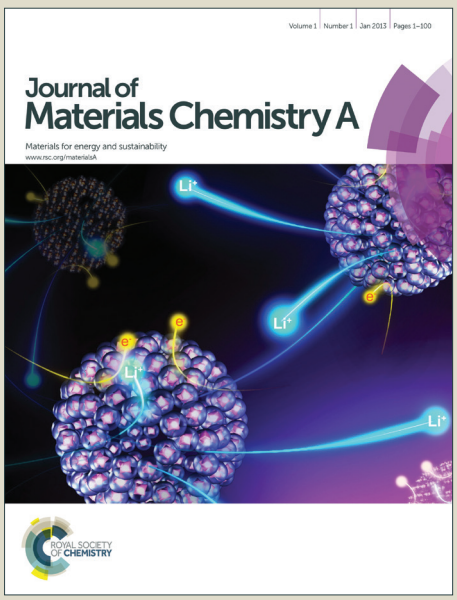

ROYAL SOCIETY OF CHEMISTRY

www.rsc.org/materialsA

Journal of Materials Chemistry A RSCPublishing

PAPER

Compressed hydrogen gas-induced synthesis of Au-Pt core/shell nanoparticle chains towards high-performance catalysts for Li-O_2 batteries

Cite this: DOI: 10.1039/x0xx00000x

Received 00th January 2014,
Accepted 00th January 2014

DOI: 10.1039/x0xx00000x

www.rsc.org/

Cheng Chao Li,‡[a] Wenyu Zhang,‡[ac] Huixiang Ang,[a] Hong Yu,[ac] Bao Yu Xia,[b] Xin Wang,[b] Yan Hui Yang,[b] Yang Zhao,[a] Huey Hoon Hng*[a] and Qingyu Yan*[acd]

Herein, we reported a green synthetic route for Au-Pt core/shell nanoparticle chains by a two-step route without any usage of surfactant. In the synthesis, compressed hydrogen was used as a reducing reagent, which also promotes assembly of the particle chains. As-prepared monodisperse gold nanoparticles were manipulated by dipoles to form chain-like nanostrucutures under high pressure; meanwhile, in situ epitaxial growth of Pt shell on gold nanochains took place, leading to the formation of Au-Pt core/shell nanoparticle chains. The resulting bimetallic Au-Pt core/shell chains showed an excellent catalytic activity as cathodes in lithium oxygen batteries with a low charge-discharge over potential and outstanding cycle performance due to its clean catalytic surface, interconnected nanostructure as good electron path and innate synergistic effect.

Introduction

As one of important energy conversion technologies, rechargeable Li-oxygen batteries have attracted great interest because they potentially have much higher gravimetric energy storage density compared with all other chemical batteries and compatible with gasoline.[1-6] In addition, Li-oxygen batteries are also an eco-friendly electrochemical power sources as it uses oxygen from the environment as the cathode material. However, the practical use of Li-O_2 batteries are still blocked by several serious drawbacks, including high charge-discharge over-potential, low rate capability, and poor cycling stability.[7-10] It is generally considered that the key factor to improve the electrochemical performance of Li-O_2 batteries is to find effective cathode catalysts to promote the oxygen reduction (ORR) and oxygen evolution reactions (OER).[11-14] To this end, Tremendous efforts have been devoted to explore various cathode catalysts to address the above challenges.[15-18] Especially, bifunctional catalysts such as Fe–N–C,[19] transition bimetallic nitrides,[20] α-MnO_2/Pd,[21] porous carbon or two-dimensional (2D) graphene nanosheet (GNS)-supported transition metal oxides[22] have also received great interest owing to their favorable ORR and OER activities. Shao-Horn and co-workers reported a new bifunctional catalyst Pt-Au alloy for rechargeable Li-oxygen batteries using carbonate electrolyte.[23] The new bifunctional Pt-Au electrocatalyst significantly decreases the overvoltage, especially for the charge process. However, the Pt-Au electrocatalyst based cells suffer from sever degradation of carbonate electrolytes.[24] Though ether solvents have been demonstrated as an effective alternative for carbonate based electrolytes and much progress has been achieved, it still remains a great challenge to explore novel bifunctional electrocatalysts to upgrade the performance of Li-O_2 cells.

As we know, the size, morphology and composition of catalyst particles on the nanometer scale profoundly affect their reaction performance. Nanoscaled catalytst particles with large specific surface area would lead to abundance active sites involved in the catalytic reactions.[25-29] In particular, the controls on catalyst particle morphology allow a selective exposure of a larger fraction of the reactive facets on which the active sites can be enriched and tuned. Recent theoretical calculation based on first-principle demonstrated that the activity of ORR/OER catalysts is also greatly dependent on the electron transfer efficiency.[30] Sufficient electron participation can quickly reduce adsorbed oxygen molecules to OH^- without any barrier through an efficient $4e^-$ pathway.[30] Compared to separated metal nanoparticle catalysts, interconnected metal nanoparticles, e.g. chains, would have better electron transfer efficiency. Therefore, it is highly desirable but challenging to develop a synthetic route for precious metal-based bifunctional catalysts with interconnected structure and clean catalytic surface.

In this study, we reported a green synthetic process to prepare Au-Pt core/shell nanoparticle chains by integration of electrical dipole-induced self-assembly and simultaneous epitaxial growth of Pt shell. Compressed hydrogen acted as a clean reducing reagent and in the synthesis, which also help the

assembly of the nanoparticles. As expected, the obtained bimetallic Au-Pt core/shell nanoparticle chains showed excellent catalytic activity and stability as cathodes in non-aqueous lithium oxygen batteries due to their clean catalytic surface and interconnect nanostructure. At a current density of 200 mAg^{-1}, the fabricated Li-O_2 cell operating with an ether-based electrolyte exhibits a discharging voltage of ~2.7 V and a charging voltage of 4.0 V for 20 cycles.

Results and discussion

The compressed hydrogen gas-induced self-assembly and growth method for preparing Au/Pt core/shell nanoparticle chains is shown schematically in Figure 1. The virtue of this method for preparing core–shell nanomaterials is that the shell thickness/coverage can be easily controlled by simply adjusting the dosage of the second metal ions (Pt) to Au seeds in solution. At a lower concentration of H_2PtCl_4, Pt^0 can be only deposited on Au core to form monodisperse Au/Pt core/shell nanoparticles by heterogeneous nucleation growth. Further increase of the concentration of H_2PtCl_4 will allow more Pt^0 to deposit on Au core and connect the neighbouring Au nanoparticles to form chains. Recently, various routes, involving surfactant-based templates,[32] molecular recognition,[33] specific functionalization,[34] surface- or solvent-induced phase separation[35] and magnetic dipoles,[36] have been developed to assemble pre-synthesized metallic nanoparticles into one-dimensional chains and networks that have potential applications in sub-wavelength optical and thermal devices. In this work, compressed hydrogen is used as the driving force for producing such elegant assembled nanochain networks through unbalancing the attractive van der Waals potentials and the residual electrostatic repulsions and increase the chance of Brownian collisions. The calculated energy of dipole attraction between nanoparticles can be as high as 10 kJ/mole based on the classical formula ($E = -\frac{\mu^2}{2\pi\varepsilon_0 r(r^2 - d_{Np}{}^2)}$, $\varepsilon_0 = 8.85 * 10^{-12} C^2 J^{-1} m^{-1}$) .[37] Without pressure involved, the gold nanoparticles system is relatively stable due to the surface charge induced electrostatic repulsions counteracts the attractive van der Waals and hydrogen bonding potentials. However, after high pressure (~250-500 PSI) is introduced into the reactor, hydrogen-expanded aqueous solution will reduce the solvating ability to sodium citrate. Partial loss of the surface-adsorbed charged citrate ions, which reduces the electrostatic repulsions between the particles. The nanoparticles under the influence of serendipitous Brownian collisions and attractive van der Waals force may start to form close contact. Dipole-dipole interactions then trigger the formation of linear chains of single nanoparticles to minimize enthalpy of the system by promoting dipole alignment and reducing inter-dipole distances. Simultaneously, Pt precursor $PtCl_4^{2-}$ could be reduced by compressed hydrogen gas and slowly deposit on interconnected gold nanoparticles, resulting in final Au-Pt core/shell nanoparticle chains.

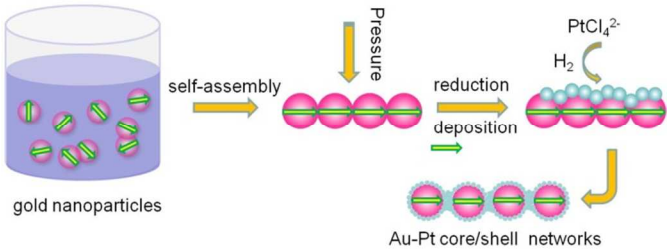

Figure 1. The schematic model diagram for Au-Pt core/shell nanoparticle chains; the arrow is the electrical dipoles. The Pt shell is thin and highly porous.

Figure 2 shows the X-ray diffraction (XRD) pattern of as-prepared samples. Two sets of diffraction peaks were clearly observed, which can be indexed to the (111), (200), and (220) reflections of face-centered cubic Pt (JCPDS #04-0802) and Au (JCPDS #04-0784), respectively. All diffraction peaks are broadened, indicating nanoscale crystal domain size. The peak split of Au and Pt phase suggests that the product is heterogeneous phases but solid solution, which is in agreement with the previously reported powder diffraction results.[23,38]

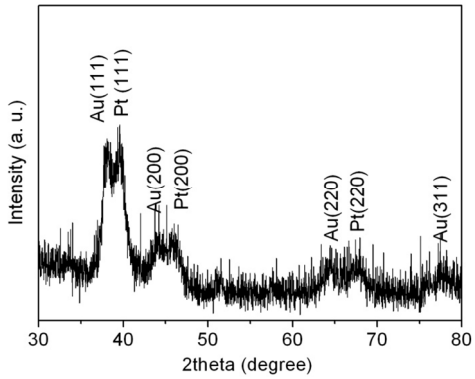

Figure 2. XRD pattern of Au-Pt core/shell nanoparticle chains.

Transmission electron microscopy (TEM) was further used to characterize the morphology and detailed structure of the products. Figure 3a is the TEM images of gold nanoparticles prepared by sodium citrate reduction. It can be seen that the gold nanoparticles are mondisperse with an averaged particle size of 15 nm. After hydrogen induced reduction process in the present of H_2PtCl_4 precursor, chain-like products were obtained (Figure 3b and c). As can be seen from the TEM image, the nanoparticles connect each other to form linear assembly with observable sub branches. It should be noticed that there is no gap between adjacent nanoparticles (Figure 3d and e), which is quite different from previously reported metal nanoparticle chains governed by electrostatic force, surfactants and magnetic force.[39-41] The high-resolution TEM image (Figure 3f) indicate that the gold nanoparticles were linked and coated by thin Pt shells to form a bean pod-like structure. The observed lattice spacing of 2.30 Å corresponds to the (111) facet of face-centered cubic (fcc) Pt.The core/shell structure was confirmed by electron energy-loss spectrum (EELS) mapping analysis. Figure SI-1 shows EELS mapped images of Au/Pt nanoparticles, in which Au

and Pt are color-coded green and red, respectively. Au is present only in the core region of each nanoparticle, but Pt only on the shell.

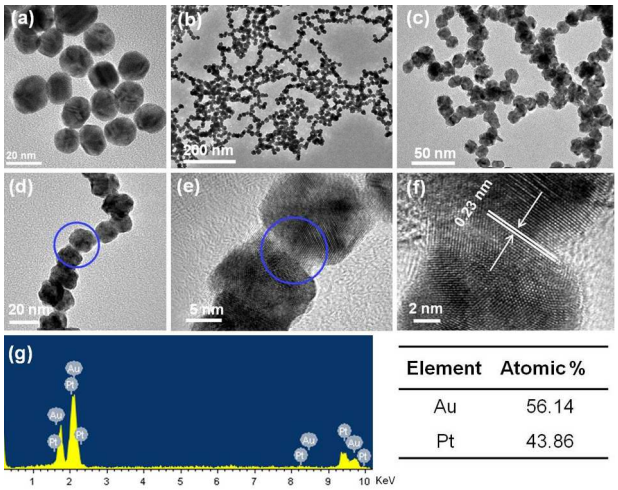

Figure 3. RepresentativeTEM images of (a) gold nanoparticles, (b, c) Au-Pt core/shell nanoparticle chains, (d) A single Au-Pt nanochain. (e, f) HRTEM images of the Au-Pt core/shell nanochain. (g) EDX spectrum of Au-Pt core/shell nanoparticle chains.

The line-scanned EELS data of a single nanoparticle (Figure SI-1) further confirmed the core-shell structure showing Au inside, Pt outside. The energy dispersive X-ray spectrometry (EDX) was performed on a random selected area of the sample, showing the Au and Pt core/shell network-like products are composed only of gold and platinum (Figure 3g). The contents of Au and Pt are 56.14 at% and 43.86 at%, respectively, which is close to that of precursor solution.

Figure 4 shows the cyclic voltammetry (CV) profiles of the as-prepared Au-Pt core/shell in 0.5 M H_2SO_4 electrolyte. As shown in Figure 4, there are well-defined hydrogen desorption/adsorption peaks between -0.24-0.2 V and Pt oxidation/reduction peaks in the range of 0.2-1.0 V. The electrochemically active surface areas (ECSA) were calculated

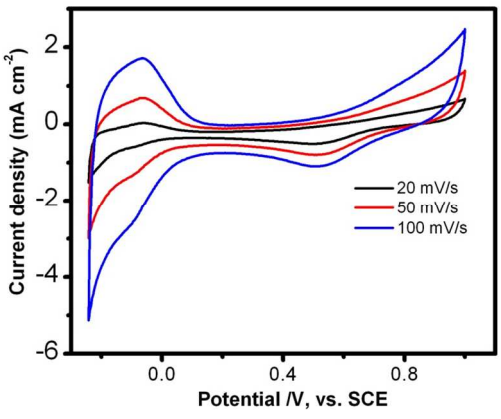

Figure 4. Cyclic voltammetric curves of Au-Pt core/shell nanoparticle chains recorded in 0.5M H_2SO_4 solution at different scan rate.

by measuring the coulombic charge of hydrogen adsorption and assuming a value of 210 μC/cm^2 for the adsorption of a hydrogen monolayer. The ECSA were calculated to be 25.8 m^2/g. The lower ECSA for the Au/Pt core/shell nanoparticle chains catalyst, compared with Pt nanoparticles in commercial catalysts (ECSA, 51.0 m^2/g), is most likely due to its larger

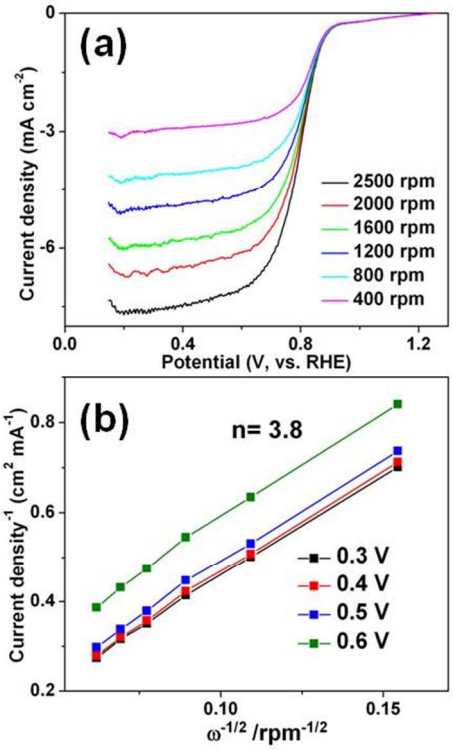

Figure 5. (a) Linear sweep voltammetry curves of ORR at various rotation rates for Au-Pt core/shell nanoparticle chains modified electrode. (b) Koutecky-Levich plots of Au-Pt core/shell nanoparticle chains electrode derived from RDE voltammograms in (a) at different electrode potentials.

size. The oxygen reduction reaction (ORR) activity of Au-Pt core/shell nanoparticle chains was investigated using rotating-disk electrode (RDE) technique at a scan rate of 10 mVs^{-1} (Figure 5a). From the RDE curves, The ORR current densities increased with the rotation speed increasing, indicating it is a diffusion controlled process. The current densities at 0.40 V are 4.6 mAcm^{-2} and the half-wave potential of Au-Pt core/shell nanoparticle chains is 0.825 V at a rotation speed of 1600 rpm. Obviously, the activity is much better than commercial Pt/C catalyst (0.818 V). The RDE polarization curves of oxygen reduction recorded at different rotation speeds (400 to 2500 rpm) were also analyzed using the Koutecky-Levich (K-L) equation (Figure 5b).[42]

$$\frac{1}{J}=\frac{1}{J_k}+\frac{1}{J_L}=\frac{1}{0.62nFC_0D^{2/3}v^{-/6}\omega^{1/2}}+\frac{1}{nFkC_0}$$

Where, J is the measured current density, and J_k and J_L are the kinetic and diffusion limited current densities, respectively; n is overall number of electrons transferred per oxygen molecule during ORR; F is Faraday's constant, C_0 is the concentration of dissolved oxygen (1.2×10^{-6} mol cm^{-3}), D is the diffusion

coefficient of oxygen (1.9×10^{-5} cm^2s^{-1}), v is the kinetic viscosity of solution and k is the apparent electron transfer rate constant. The parallel fitting lines of the K-L plots at various electrode potentials (0.3-0.6V) show good linearity and parallelism, indicating that the ORR process over the Au-Pt core/shell nanoparticle chains catalyst follows first-order kinetics with respect to the concentration of oxygen. The electron transfer number (n) per O_2 molecule is evaluated to be 3.8 for the Au-Pt core/shell nanoparticle chains modified-electrode. These results suggest an apparent quasi-four-electron oxygen reduction process. In other words, O_2 can be dominantly reduced to hydroxide ions at these potentials, which is desirable for achieving highly efficient electrocatalytic ORR.

To investigate the electrochemical performances, Li-oxygen batteries in a nonaqueous electrolyte were fabricated. Our Li–O_2 cell was assembled with modified Swagelok configurations,[43] in which Li foils are used as the reference and counter electrodes and the stainless steel net supported Au-Pt/C as the working electrodes. The specific discharge-charge capacities are limited to 1000 $mAhg^{-1}$. Typical charge and discharge voltage profiles of the Li-O_2 cell are shown in Figure 6a. At a current density of 50 mAg^{-1} based on the total mass of the Au-Pt core/shell network-carbon hybrid material, the average discharging voltage was about 2.82 V, close to the thermodynamic potential of the reaction $2\,Li^+ + 2e^- + O_2 \rightarrow Li_2O_2$, while the average charging voltage was about 3.77 V, 0.82 V higher than the discharging voltage. This overpotential was much lower than those of other reported catalysts such as graphene,[44] transition metal oxides,[45] perovskite oxides,[16] MoN–graphene[8] and mesoporous pyrochlore.[46] The overpotential slightly increased with increasing current densities (Figure 6a), but the charging potential at 100 and 200 mA g^{-1} was still < 4.0 V. The round-trip efficiencies (the discharging specific energies/charging specific energies) of the as-prepared Au-Pt core/shell nanoparticle chains electrode (Figure 6a), at a current densities of 50, 100 and 200 mAg^{-1}, are calculated to be 78.3%, 67.0%, and 57.1%, respectively, which are also much improved in comparison to pure carbon cathode and reported graphene materials.[42] to demonstrate the merits of core/shell chain, the lithium oxygen performances based on other Au and Pt nanostructures have also been evaluated. Clearly, the Au/Pt core/shell chains electrodes exhibit lower charge and discharge potential in comparison with monodispersed Au/Pt core/shell nanoparticles and mixture of Au Pt nanoparticles (Figure SI-3 and SI-4). Furthermore, the Au-Pt core/shell network electrodes also exhibit good cycling stability. Cycle life of the Li-O_2 cell was tested with a capacity cut-off of 1000 $mAhg^{-1}$ at a current density of 200 mAg^{-1}. The cell showed good cycling ability over 20 cycles in dry oxygen (Figure 6c). During cycling, the final voltage of each discharging segment stabilized at 2.6 to 2.7 V, and the final voltage of each charging segment was in the range of 4.0 to 4.1V (Figure 6b and c). The good cycling performance of the Au-Pt core/shell network electrode can be attributed to the interconnected bimetal nanostructures, which greatly increase the electron transportation in the electrocatalysts compared to separated precious metal nanoparticles (Figure SI-5). Particularly, the bimetallic catalysts not only inherit the catalytic properties of each component, but also have higher catalytic efficiencies than their monometallic counterparts, owing to strong synergy between the metals. The origin of the synergy between two metals is generally ascribed to electronic (ligand) and geometric (ensemble) effects. In the gold bimetallic catalysts, since gold has the highest electronegativity (2.54), electron transfer from the second metal to gold may occur, which will affect the catalytic performance of gold by electronic modification. In addition, the synthesis route eliminates usage of strong coordinated surfactants, which results in a clean catalytic surface.

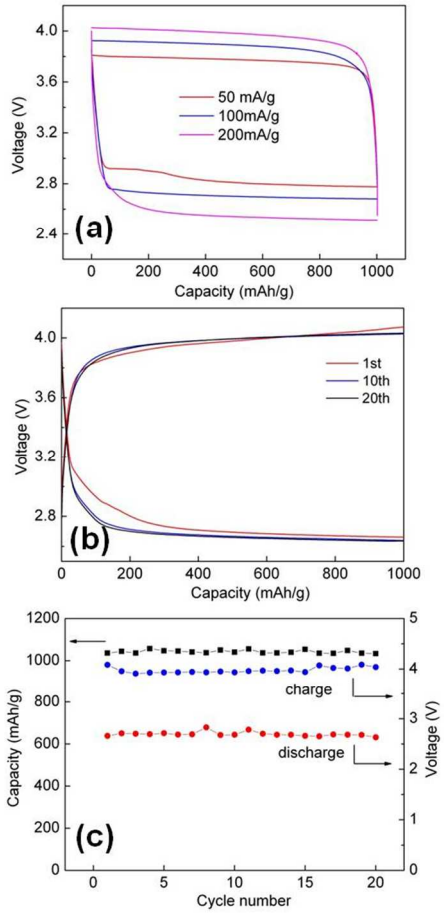

Figure 6. (a) Charging and discharging voltage profiles of the cell at various current densities. (b) Charging and discharging voltage profiles of the cell at 200 mA/g. (c) Specific discharge capacity of the cell over 20 cycles at 200 mA/g (black) and Cell voltage upon completion of each discharge (red) and charge (blue) segment over the 20 cycles.

Conclusions

A green synthetic process was developed to prepare Au-Pt core/shell nanoparticle chains bifunctional electrocatalysts using high pressure hydrogen gas as self-assembly inducing reagent and reducing reagent. In the synthesis, no surfactants

were used and the electrical dipoles were believed to be the driving force for producing such elegant assembled nanochain networks. Due to its clean catalytic surface and improved electron transfer efficiency, the obtained bimetallic Au-Pt core/shell nanoparticle chains showed an excellent catalytic activity as cathodes in lithium oxygen batteries with a low charge-discharge over potential and outstanding cycle performance interconnect nanostructure.

Experimental

Synthesis of gold nanoparticles

The gold nanoparticles were synthesized according to the route reported previously with minor modification.[31] In a typical synthesis, 1.67 mL of 30 mM $HAuCl_4$ aqueous solution was added rapidly to a solution of 4 mM sodium citrate (50 mL) that was heated under reflux. Heating under reflux was continued for an additional 15 min, during which time the colour changed to deep red. The obtained gold nanoparticles suspension was cooled down to room temperature automatically and stored for further usage.

Synthesis of Au-Pt core/shell nanoparticle chains

Under vigorous stirring, 0.5 mL of 30 mM H_2PtCl_4 was added into 20 mL gold nanoparticles suspension. The mixture was then transferred into a parr reactor with a volume of 30 mL. The reactor was firstly purged with hydrogen gas for three times to remove air. Compressed hydrogen gas was then introduced into the reactor (the pressure can be controlled by regulator). The reaction system was kept at room temperature for 24 h. After that, the hydrogen was released and the black product was collected by centrifugation and washed with deionized water and absolute ethanol several times, followed by freeze drying.

Electrocatalytic activity measurement

Electrocatalytic activities of sample were measured in a conventional three electrode cell using Autolab potentiostat/galvanostat (Model PGSTAT-72637, Brinkman Instruments). The three-electrode cell consisted of a Pt wire serving as the counter electrode, a saturated calomel electrode (SCE) serving as the reference electrode, and a glassy carbon (GC) disk (5 mm in diameter), coated with catalysts, serving as the working electrode. To fabricate a working electrode, 5 mg of catalyst powder was dispersed in a diluted Nafion solution with ultrasonication for 30 min to form a homogeneous black suspension. Then 10 μL of the resulting suspension was carefully pipetted onto the GC electrode surface, and the coating was dried at room temperature for 12 h.

Electrochemical testing of Li-O_2 cells

The oxygen electrodes were prepared as follows: Catalyst slurry was prepared by mixing the as-prepared Au-Pt catalyst (40 wt%), super P (40%) and Polyvinylidene fluoride (PVDF) (20 wt%) in N-Methyl-2-pyrrolidone (NMP). The mixture was then coated on a glass fiber separator, which was punched into discs with a diameter of 14 mm and dried at 80 ^oC in a vacuum oven for 12 h. The typical loading of the air electrode is about 1 mg cm^{-2}. The Li-O_2 cells were assembled in an Ar filled glove box with water and oxygen level less than 0.1 ppm. A lithium foil was used as the anode and was separated by one glass microfibre filters, soaked in 1 M $LiCF_3SO_3$ in tetra(ethylene) glycol dimethyl ether (TEGDME) as the electrolyte. Li-O_2 cells were assembled in the following order:[23] 1) placing a lithium foil onto the bottom of stainless steel cell, which is used as current collector, 2) adding 0.2 mL electrolyte, 3) placing one pieces of the separator onto the lithium foil, 4) adding more electrolyte, 5) placing the cathode-coated separator onto the separator, 6) adding on top a cathode current collector and 7) purging the cell with pure oxygen for 2 minutes.The cell was gas-tight except for the stainless steel mesh window that exposed the porous cathode film to the oxygen atmosphere. All measurements were conducted in 1 atm dry oxygen atmosphere to avoid any negative effects of humidity and CO_2. Galvanostatic discharg-charge was conducted on a Neware battery testing system. The specific capacity was calculated based on the mass of Super-P carbon black in the cathode electrodes

Characterization

Crystallographic phases of the prepared products were investigated by X-ray power diffraction method (XRD) using Shimadzu XRD-6000 with Cu Kα radiation. The morphologies of the as-prepared sample were characterized by a field-emission scanning electron microscopy (FESEM; JSM-6700F), transmission electron microscopy (TEM; JEM-2010, 200 kV), selected area electron diffraction (SAED), and high-resolution transmission electron microscopy (HRTEM; JEM-2010F, 200 kV).

Acknowledgements

The authors gratefully acknowledge AcRF Tier 1 RG 2/13 of MOE (Singapore), A*STAR SERC grant 1021700144, Singapore MPA 23/04.15.03 RDP 020/10/113 grant and Singapore National Research Foundation through the Competitive Research Programme (Project No. NRF-CRP5-2009-04).

Notes and references

[a]School of Materials Science and Engineering, Nanyang Technological University, 639798, Singapore, [b]School of Chemical and Biomedical Engineering, Nanyang Technological University, 637457, Singapore; [c]TUM CREATE Research Centre@NTU, Nanyang Technological University, 637459, Singapore,; [d]Energy Research Institute@NTU, Nanyang Technological University, 637553, Singapore
E-mail: ashhhng@ntu.edu.sg; alexyan@ntu.edu.sg;
Fax: +65 6790 9081; Tel: +65 6790 4583
‡The authors contributed equally to this work.
Electronic Supplementary Information (ESI) available: [details of any supplementary information available should be included here]. See DOI: 10.1039/b000000x/

1. J. S. Lee, S. T. Kim, R. Cao, N. S. Choi, M. Liu, K. T. Lee, J. Cho, *Adv. Energy Mater.*, **2011**, 1, 34.

2. H. Lim, K. Park, H. Song, E. Y. Jang, H. Gwon, J. Kim, Y. H. Kim, M. D. Lima, R. O. Robles, X. Lepró, R. H. Baughman, K. Kang, *Adv. Mater.,* **2013**, 25, 1348.
3. Y. L. Li, J. J. Wang, X. F. Li, D. S. Geng, R. Y. Li, X. L. Sun, *Chem. Commun.,* **2011**, 47, 9438.
4. J. M. Tarascon and M. Armand, *Nature*, **2001**, 414, 359.
5. G. Girishkumar, B. McCloskey, A. C. Luntz, S. Swanson and W. Wilcke, *J. Phys. Chem. Lett.,* **2010**, 1, 2193.
6. P. G. Bruce, S. A. Freunberger, L. J. Hardwick and J.-M. Tarascon, *Nat. Mater.,* **2012**, 11, 19.
7. S. M. Dong, X. Chen, K. J. Zhang, L. Gu, L. X. Zhang, X. H. Zhou, L. F. Li, Z. H. Liu, P. X. Han, H. X. Xu, J. H. Yao, C. J. Zhang, X. Y. Zhang, C. Q. Shang, G. L. Cui and L. Q. Chen, *Chem. Commun.*, **2011**, 47, 11291.
8. S. M. Dong, X. Chen, K. J. Zhang, L. Gu, L. X. Zhang, X. H. Zhou, L. F. Li, Z. H. Liu, P. X. Han, H. X. Xu, J. H. Yao, C. J. Zhang, X. Y. Zhang, C. Q. Shang, G. L. Cui and L. Q. Chen, Chem.Commun., **2011**, 47, 11291.
9. Christensen, J. et al. A Critical Review of Li/Air Batteries. *J. Electrochem. Soc.,* **2012**, 159, R1-R30.
10. F. J. Li, T. Zhang, H. S. Zhou, *Energy Environ. Sci.*, **2013**, 6, 1125.
11. X. J. Wang, Y. Y. Hou, Y. S. Zhu, Y. P. Wu, R. Holze, *Sci. Rep.*, **2013**, 3, 1401.
12. J.-L. Shui, N. K. Karan, M. Balasubramanian, S.-Y. Li and D.-J. Liu, *J. Am. Chem. Soc.,* **2012**, 134, 16654.
13. D. Oh, J. Qi, Y. Lu, Y. Zhang, S. H. Yang, A. M. Belcher, *Nat. Commun.*, **2013**, 4, 2756.
14. Y. Y. Shao, S. Y. Park, J. Xiao, J. G. Zhang, Y. Wang, J. Liu, *ACS Nano*, **2012**, 2, 844.
15. Y. Li, M. Gong, Y. Liang, J. Feng, J. Kim, H. Wang, G. Hong, B. Zhang, H. Dai, *Nat. Commun.,* **2013**, 4, 1805.
16. J. Xu, D. Xu, Z. Wang, H. Wang, L. Zhang, X. Zhang, *Angew. Chem. Int. Ed.,* **2013**, 52, 3887-3890.
17. Thapa, A. K.; Hidaka, Y.; Hagiwara, H.; Ida, S.; Ishihara, T. *J. Electrochem. Soc.,* **2011**, 15, A1483.
18. H. L. Wang, Y. Yang, Y. Y. Liang, G. Y. Zheng, Y. G. Li, Y. Cui, H. J. Dai, *Energy Environ. Sci.,* **2012**, 5, 7931.
19. J. L. Shui, N. K. Karan, M. Balasubramanian, S. Y. Li and D. J. Liu, *J. Am. Chem. Soc.,* **2012**, 134, 16654.
20. K. Zhang, L. Zhang, X. Chen, X. He, X. Wang, S. Dong, P. Han, C. Zhang, S. Wang, L. Gu and G. Cui, *J. Phys. Chem. C*, **2013**, 117, 858.
21. Thapa, A. K.; Hidaka, Y.; Hagiwara, H.; Ida, S.; Ishihara, T. *J. Electrochem. Soc.* **2011**, 15, A1483.
22. Y. Cao, Z. Wei, J. He, J. Zang, Q. Zhang, M. Zheng and Q. Dong, *Energy Environ. Sci.,* **2012**, 5, 9765.
23. Y. C. Lu, Z. C. Xu, H. A. Gasteiger, S. Chen, K. H. Schifferli, S. H. Yang, *J. Am. Chem. Soc.*, **2010**, 132, 12170.
24. B. D. McCloskey, R. Scheffler, A. Speidel, D. S. Bethune, R. M. Shelby, A. C. Luntz, *J. Am. Chem. Soc.*,2011, 133, 18038.
25. D. Zhang, X. Du, L. Shi, R. Gao, *Dalton Trans.*, **2012**, 41, 14455.
26. L. Ruan, E. Zhu, Y. Chen, Z. Lin, X. Huang, X. Duan, Y. Huang, *Angew. Chem. Int. Ed.*, **2013**, 52, 12577.
27. D. Wang, H. L. Xin, R. Hovden, H. Wang, Y. Yu, D. A. Muller, F. J. Disalvo, H. D. Abruña, *Nat. Mater.,* **2013**, 12, 81.
28. P. Strasser, S. Koh, T. Anniyev, J. Greeley, K. More, C. Yu, Z. Liu, S. Kaya, D. Nordlund, H. Ogasawara, M. F. Toney, A. Nilsson, *Nature Chem.,* **2010**, 2, 454.
29. L. W. Su, Y. Jing. Z. Zhou, *Nanoscale*, **2011**, 3, 3967.
30. Y. Zheng, Y. Jiao, J. Chen, J. Liu, J. Liang, A. du, W. Zhang, Z. Zhu, S. C. Smith, M. Jaroniec, G. Q. Lu, S. Z. Qiao, *J. Am. Chem. Soc.*, **2011**, 133, 20116.
31. Y. Chen, C. Yu, T. Lu, W. Tseng, *Langmuir*, **2008**, 24, 3654.
32. Y. Yang, S. Matsubara, M. Nogami, J. L. Shi, W. M. Huang, *Nanotechnology*, **2006**, 17, 2821.
33. C. L. Chen, P. J. Zhang, N. L. Rosi, *J. Am. Chem. Soc.*, **2008**, 130, 13555.
34. K. G. Thomas, S. Barazzouk, B. I. Ipe, S. T. S. Joseph, P. V. Kamat, *J. Phys. Chem. B*, **2004** , 108, 13066.
35. A. M. Jackson, J. W. Myerson, F. Stellacci, *Nat. Mater.* **2004**, 3, 330.
36. M.-R. Gao, S.-R. Zhang, Y.-F. Xu, Y.-R. Zheng, J. Jiang, S. H. Yu, *Adv. Funct. Mater.*, **2013**, DOI: 10.1002/adfm.201302262.
37. Z. Y. Tang, N. A. Kotov, M. Giersig, *Science*, **2002**, 297, 237.
38. C. Liu, Y. Wei, C. Liu, K. Wang, *J. Mater. Chem.,* **2012**, 22, 4641.
39. S. Lin, M. Li, E. Dujardin, C. Girard, S. Mann, *Adv. Mater.,* **2005**, 17, 2553.
40. M. Li, S. Johnson, H. T. Guo, E. Dujardin, S. Mann, *Adv. Funct. Mater.*, **2011**, 21, 851.
41. G. A. DeVries, M. Brunnbauer, Y. Hu, A. M. Jackson, B. Long, B. T. Neltner, O. Uzun, B. H. Wunsch, F. Stellacci, *Science*, **2007** , 315 , 358
42. D.S. Yu, Q. Zhang, L. M. Dai, *J. Am. Chem. Soc.*, **2010**, 132, 15127.
43. W. Y. Zhang, J. X. Zhu, H. X. Ang, Y. Zeng, N. Xiao, Y. B. Gao, W. L. Liu, H. H. Hng, Q. Y. Yan, *Nanoscale*, **2013**, 5, 9651.
44. B. Sun, B. Wang, D. W. Su, L. D. Xiao, H. Ahn, G. X. Wang, *Carbon*, **2012**, 50, 727.
45. A. Debart, A. J. Paterson, J. Bao, P. G. Bruce, *Angew. Chem. Int. Ed.,* **2008**, 47, 4521.
46. S. H. Oh, R. Black, E. Pomerantseva, J. Lee, L. F. Nazar, *Nat. Chem.,* **2012**, 4, 1004.